

GaN-based vertical-cavity laser performance improvements using tunnel-junction-cascaded active regions

Joachim Piprek^{a)}

NUSOD Institute LLC, P.O. Box 7204, Newark, Delaware 19714, USA

(Received 23 May 2014; accepted 25 June 2014; published online 8 July 2014)

This Letter investigates the output power enhancement achieved by tunnel junction insertion into the InGaN multi-quantum well (MQW) active region of a 410 nm vertical-cavity surface-emitting laser which enables the repeated use of carriers for light generation (carrier recycling). While the number of quantum wells remains unchanged, the tunnel junction eliminates absorption caused by the non-uniform MQW carrier distribution. The thermal resistance drops and the excess bias lead to a surprisingly small rise in self-heating. © 2014 AIP Publishing LLC.

[<http://dx.doi.org/10.1063/1.4887377>]

Similar to widely used GaAs-based vertical-cavity surface-emitting lasers (VCSELs), GaN-based VCSELs are expected to show various advantages over their edge-emitting counterparts, including lower manufacturing costs, circular and low-divergence output beam, single longitudinal mode emission, low threshold, high-speed modulation, high-density two-dimensional arrays, wafer-level testing, and longer lifetime.¹ Potential applications of GaN-VCSELs include laser display, solid-state lighting, high-density optical data storage, high-resolution printing, low-cost optical communication, and bio-sampling. However, in contrast to the success of GaN-based edge-emitting lasers in recent years, GaN-VCSELs still face significant challenges.² One of the key material problems is the poor quality of AlGaN-based distributed Bragg reflectors (DBRs) due to the large lattice mismatch of GaN and AlN. A possible solution is the use of one or two dielectric DBRs. However, the employment of dielectric DBRs on both sides of the VCSEL cavity requires the removal of the majority of the substrate combined with a precise control of the remaining cavity length.³

The first continuous-wave (CW) operation of a current-injected GaN-VCSEL was demonstrated in 2008 at the low temperature of 77 K utilizing an undoped AlN/GaN DBR at the bottom with superlattice interlayers for strain relaxation and a Ta₂O₅/SiO₂ dielectric DBR at the top.⁴ An AlGaN electron blocker layer (EBL) was later added and led to CW lasing at room temperature with a maximum output power of 37 μW.⁵ A key design feature of this hybrid VCSEL is the thick multi-quantum well (MQW) active region with ten QWs covering an entire period of the standing wave and thus avoiding the common problem of positioning the active layers at an optical intensity peak (Fig. 1). However, our analysis of this device reveals a strongly non-uniform MQW carrier density so that only the p-side QWs deliver optical gain while the n-side QWs cause optical loss (Fig. 1).⁶ Such non-uniform carrier distribution is typical for InGaN MQWs and was experimentally verified with InGaN/GaN light emitting diodes (LEDs).⁷

A possible solution to this problem is the insertion of a GaN-based tunnel junction into the MQW active region.

Such bipolar cascade (BC) designs were demonstrated in the past for GaAs- and InP-based VCSELs.^{8,9} Previously reported GaN-VCSELs feature tunnel junctions only on the p-doped side for improved hole injection into the active region.¹⁰ However, the recent demonstration of low-resistance GaN-based tunnel junctions¹¹ triggered promising investigations into high-efficiency blue LEDs using bipolar cascade structures.^{11–13} GaN-based BC-LEDs were earlier fabricated for dual-wavelength applications, employing two different active regions.¹⁴

Motivated by these reports on GaN-based BC-LEDs, we here demonstrate the application of the bipolar cascade concept to GaN-based VCSELs using the cited hybrid VCSEL as a starting point. In combination with published measurements, we utilize numerical simulation to analyze performance limiting physical mechanisms, in particular the non-uniform MQW carrier distribution. We show that the insertion of a tunnel junction into the MQW eliminates this problem and allows for double the output power without causing significantly more self-heating.

Numerical simulation is a popular tool to analyze the complex interactions of electronic, photonic, and thermal processes in VCSELs.^{15–17} We here employ a modified version of the

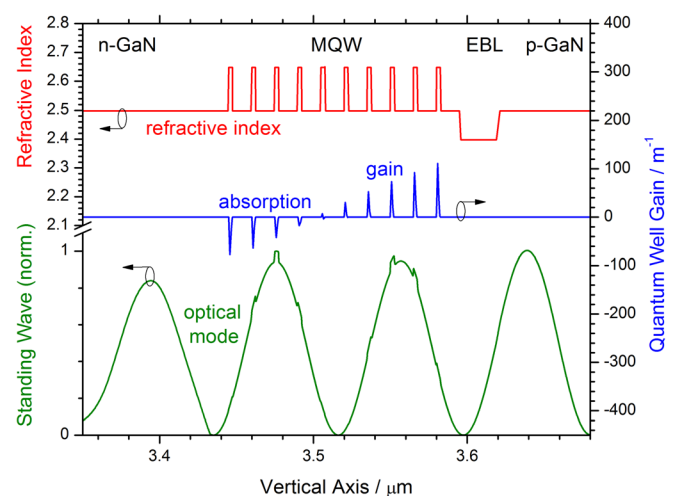


FIG. 1. Vertical profiles calculated for the original GaN-VCSEL at lasing threshold.

^{a)}piprek@nusod.org

PICS3D laser simulation software.¹⁸ The three-dimensional model self-consistently computes the semiconductor carrier transport equations coupled with a quantum-mechanical representation of spontaneous and stimulated photon emission from the quantum wells. Schrödinger and Poisson equations are solved iteratively to account for the strong built-in polarization and for the quantum-confined Stark effect. The carrier transport model considers drift and diffusion of electrons and holes, Fermi statistics, thermionic emission at hetero-interfaces, as well as band-to-band tunneling. The internal heat generation is calculated self-consistently, accounting for all relevant heat sources, including Joule heat, non-radiative recombination, and Peltier heat.¹⁹ Further details of our GaN-VCSEL model are published elsewhere.²⁰ A similar model was previously employed in the analysis of high-power GaN-based edge-emitting lasers, resulting in excellent agreement with measurements.²¹

For model validation and analysis, we first simulate the CW performance of the original VCSEL according to published data.^{5,22} The $7\text{-}\lambda$ -cavity is sandwiched between an n-side 29-period AlN/GaN DBR and a p-side 10-period $\text{Ta}_2\text{O}_5/\text{SiO}_2$ dielectric DBR (λ -resonant cavity wavelength). The MQW active region comprises 10 InGaN quantum wells, each 2.5 nm thick, that are separated by 12.5-nm-wide GaN barriers. A 24-nm wide p-AlGaN EBL is grown on top of the MQW. The current is injected through a 30-nm-thick indium tin oxide (ITO) layer on the p-side ($10\text{ }\mu\text{m}$ aperture radius) and an intra-cavity ring contact on the n-side. Figure 2 shows good agreement of the calculated light-current (LI) and voltage-current (VI) characteristics with the experiments. The lasing threshold is mainly influenced by the QW Auger recombination coefficient of $10^{-31}\text{ cm}^6/\text{s}$, which is in good agreement with previous publications.²³ The VI characteristic is adjusted by the measured contact resistance of $180\text{ }\Omega$. The maximum internal temperature rise is $\Delta T = 54\text{ K}$ at 16 mA injection current resulting in a thermal device resistance of $\Delta T/IV = 470\text{ K/W}$ (I-current, V-voltage, the small light power is neglected). The thermal resistance deduced from the measured wavelength shift is

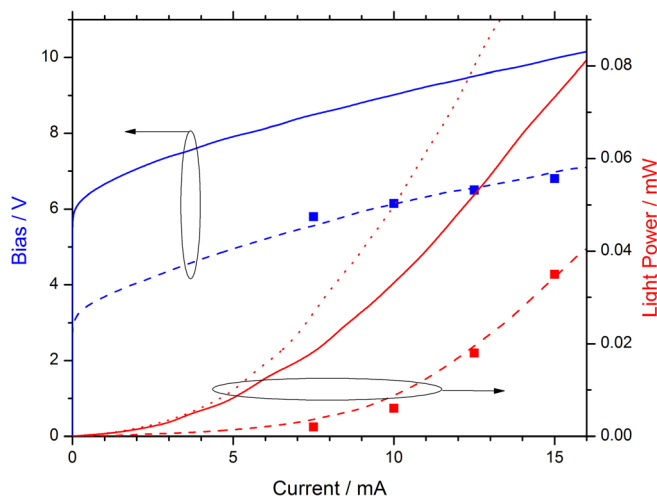


FIG. 2. Light power (red) and laser bias (blue) vs. current for the BC-VCSEL (solid) and for the original design (dashed). Squares give measured results.⁵ The dotted line shows the BC-VCSEL light output calculated without tunnel junction absorption.

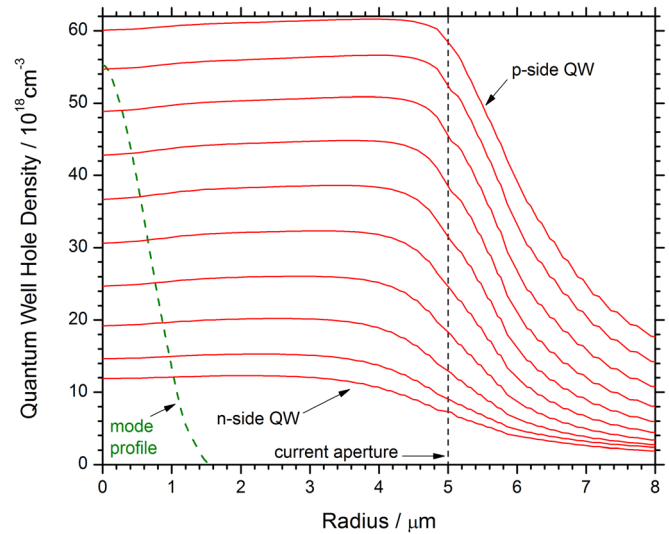


FIG. 3. Lateral hole density profiles inside each of the 10 quantum wells of the original device at lasing threshold. The dashed line indicates the mode profile (a.u.).

somewhat smaller (380 K/W) because it is based on the average cavity temperature.²²

According to experimental observations, a $3\text{-}\mu\text{m}$ -wide fundamental lasing mode is considered in this simulation. Figure 3 plots the radial mode profile as well as the radial hole density profile for all ten quantum wells as calculated near threshold. The almost uniform hole injection through the ITO contact layer prevents current crowding and supports a fundamental lasing mode near the center of the aperture, in agreement with measurements.⁵ However, the current aperture is much wider than the optical mode, and most of the injected current remains unused, which contributes to the poor performance of the original VCSEL. In vertical direction, the QW carrier density is strongly non-uniform in Fig. 3, because holes cannot move as easily across the InGaN MQW as electrons. The carrier density within the first few quantum wells on the n-doped side remains below the QW transparency density, causing the negative gain in Fig. 1.

We now insert a tunnel junction into the MQW active region of this device. GaN-based tunnel-junctions with a resistivity as low as $5.7 \times 10^{-4}\text{ }\Omega\text{ cm}^2$ were recently achieved using GdN nano-islands.¹¹ The corresponding tunneling process is difficult to simulate accurately, not only because of unknown properties of the GdN islands but also because the tunnel probability is generally very sensitive to the actual doping profile, which is unknown. To still accomplish a sufficiently realistic representation of this tunnel junction in our model, we consider a step-doped homo-junction ($15\text{ nm } 5 \times 10^{19}\text{ cm}^{-3}\text{ n}^{++}\text{GaN}/15\text{ nm } 5 \times 10^{19}\text{ cm}^{-3}\text{ p}^{++}\text{GaN}$)¹¹ and adjust the effective tunneling mass in the common WKB approximation²⁴ to reproduce the measured reverse tunnel junction resistivity.

The tunnel junction is placed at the standing wave minimum of the VCSEL to reduce the impact of the strong material absorption ($125/\text{cm}$).²⁵ The optical distance of the two MQW sets is $\lambda/2$, to maintain the overlap with the standing wave. Figure 4 shows the energy band diagram of this bipolar cascade structure as well as the gain profile. In contrast to

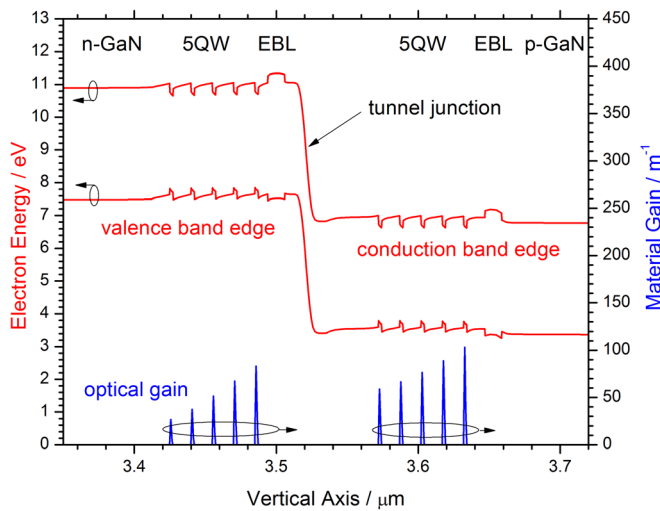


FIG. 4. Energy band diagram and optical gain for two sets of five InGaN quantum wells separated by a GaN tunnel junction.

the original device, optical gain is now provided by all quantum wells. The inclusion of an EBL at each stage is essential to limit electron leakage, but we reduce the EBL thickness to decrease the excess bias. The stimulated photon generation in this structure works as follows. Conduction band electrons are injected from the left-hand side and recombine with valence band holes inside the first QW set. The influx of new holes into these QWs can also be seen as electrons moving inside the valence band to the tunnel junction. The tunnel junction transfers these electrons into the conduction band of the second stage. The photon generation process is then repeated in the second QW set.

Figure 2 shows that our BC-VCSEL design reduces the threshold current and doubles the output power at 16 mA. The dotted line illustrates the still significant impact of tunnel junction absorption. The bias rises by about 3 V corresponding to the additional band gap. The tunnel junction resistance also causes some excess bias which is almost compensated for by the reduced EBL resistance. However, the higher bias does not translate into proportionally stronger

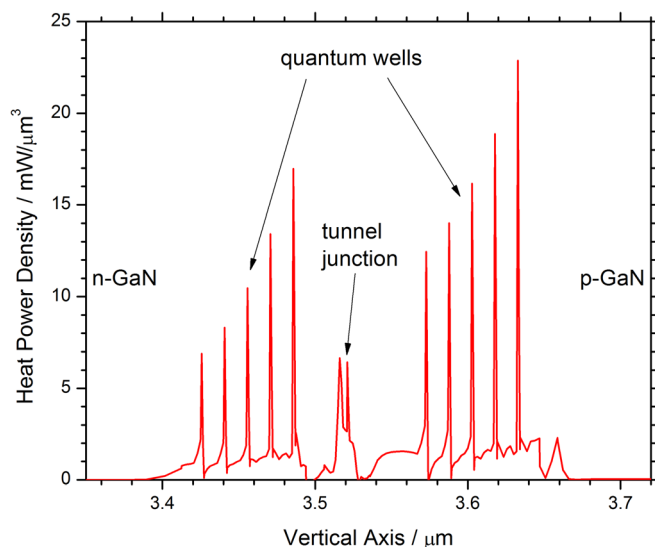


FIG. 5. Heat generation profile in the center of the BC-VCSEL at 16 mA.

self-heating. Injected electrons give up part of their excess energy by photon emission. Additional heat is mainly generated by stronger non-radiative recombination in the first five QWs, due to the higher carrier density. Joule and Peltier heat are the dominating heat sources at the tunnel junction. The calculated heat power profile in Fig. 5 verifies that the heat generated at the tunnel junction is considerably smaller than the heat from non-radiative recombination inside the quantum wells. The maximum internal temperature rise at 16 mA is $\Delta T = 60$ K, only 6° higher than before. This is also attributed to the further separation of heat sources and the improved heat dissipation enabled by the GaN spacer layer between the two QW sets. The thermal resistance consequently drops to $\Delta T/IV = 375$ K/W.

For proper comparison, the cavity wavelength is kept at 410 nm so that the gain peak offset is about the same in both cases. The measured thermal wavelength shift of 0.01 nm/K is translated into a thermal enhancement of the refractive index in each layer and leads to a very small emission wavelength shift of about 0.4 nm at 16 mA, based on the average cavity temperature. The red-shift of the gain peak is much stronger, and it is caused by self-heating as well as by the band gap renormalization due to many body effects.⁶ Figure 6 compares the net modal gain spectra. Due to tunnel junction absorption, the BC-VCSEL requires higher MQW gain than the original device, but the threshold current is still lower with the BC-VCSEL design because of the more uniform MQW carrier and gain distribution and because each carrier gets two chances to provide optical gain. Adding more tunnel junctions and QW sets is expected to further improve the VCSEL performance.⁹

In summary, we have utilized advanced numerical laser simulation to reveal performance limiting mechanisms in GaN-VCSELs based on published experimental results. The strongly non-uniform carrier distribution in the MQW active regions causes substantial absorption in n-side quantum wells. This problem is eliminated by proper insertion of a tunnel junction which leads to significant output power enhancements. The simultaneous rise in device bias does not

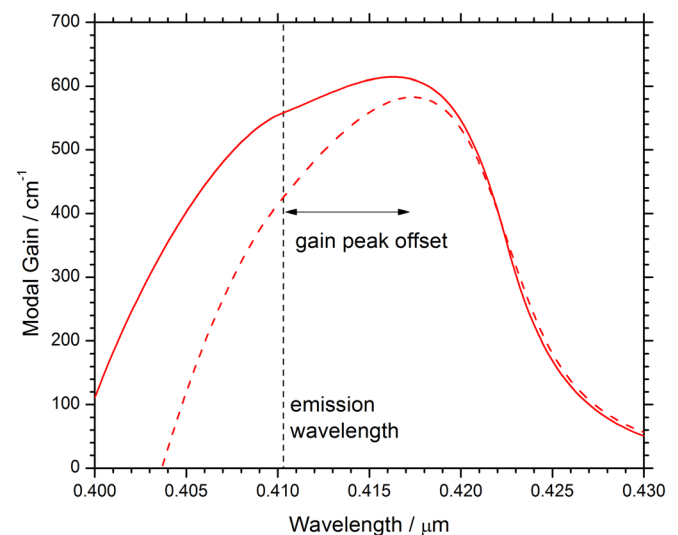


FIG. 6. Net modal gain spectrum at 16 mA for the original device (dashed) and for the BC-VCSEL design (solid). The vertical line indicates the emission wavelength.

cause a proportional increase in self-heating and the thermal resistance is smaller than before.

- ¹VCSELs, edited by R. Michalzik (Springer, Berlin, 2013).
- ²S. C. Wang, T. C. Lu, and H. C. Kuo, "GaN-based VCSELs," in *VCSELs*, edited by R. Michalzik (Springer, Berlin, 2013), Chap. 13.
- ³C. Holder, J. S. Speck, S. P. DenBaars, S. Nakamura, and D. Feezell, *Appl. Phys. Express* **5**, 092104 (2012).
- ⁴T. C. Lu, C. C. Kao, H. C. Kuo, G. S. Huang, and S. C. Wang, *Appl. Phys. Lett.* **92**, 141102 (2008).
- ⁵T. C. Lu, S. W. Chen, T. T. Wu, P. M. Tu, C. K. Chen, C. H. Chen, Z. Y. Li, H. C. Kuo, and S. C. Wang, *Appl. Phys. Lett.* **97**, 071114 (2010).
- ⁶J. Piprek, in *Proceedings of the 13th NUSOD Conference, Vancouver, Canada, 2013* (IEEE, Piscataway, 2013), pp. 89–90.
- ⁷A. David, M. J. Grundmann, J. F. Kaeding, N. F. Gardner, T. G. Mihopoulos, and M. R. Krames, *Appl. Phys. Lett.* **92**, 053502 (2008).
- ⁸J. K. Kim, S. Nakagawa, E. Hall, and L. A. Coldren, *Appl. Phys. Lett.* **77**, 3137 (2000).
- ⁹Th. Knödl, M. Golling, A. Straub, R. Jäger, R. Michalzik, and K. J. Ebeling, *IEEE J. Sel. Top. Quantum Electron.* **9**, 1406 (2003).
- ¹⁰S. R. Jeon, M. S. Cho, M. A. Yu, and G. M. Yang, *IEEE J. Sel. Top. Quantum Electron.* **8**(4) 739–743 (2002).
- ¹¹F. Akyol, S. Krishnamoorthy, and S. Rajan, *Appl. Phys. Lett.* **103**, 081107 (2013).
- ¹²J. Piprek, *Phys. Status Solidi RRL* **8**, 424 (2014).
- ¹³M. C. Tsai, B. Leung, T. C. Hsu, and Y. K. Kuo, *J. Lightwave Technol.* **32**, 1801 (2014).
- ¹⁴I. Ozden, E. Makarona, A. V. Nurmikko, T. Takeuchi, and M. Krames, *Appl. Phys. Lett.* **79**(16), 2532–2534 (2001).
- ¹⁵M. Osinski, V. A. Smagley, G. A. Smolyakov, and P. G. Eliseev, *IEEE J. Sel. Top. Quantum Electron.* **7**, 270 (2001).
- ¹⁶M. Streiff, A. Witzig, M. Pfeiffer, P. Royo, and W. Fichtner, *IEEE J. Sel. Top. Quantum Electron.* **9**, 879 (2003).
- ¹⁷P. Debernardi, "Three-dimensional modeling of VCSELs," in *VCSELs*, edited by R. Michalzik (Springer, Berlin, 2013), Chap. 3.
- ¹⁸Z. M. Li, *PIC3D* (Crosslight Software, Inc., Vancouver, Canada, 2013).
- ¹⁹G. K. Wachutka, *IEEE Trans. Comput. Aided Des.* **9**, 1141 (1990).
- ²⁰J. Piprek, Z.-M. Li, R. Farrell, S. P. DenBaars, and S. Nakamura, "Electronic properties of InGaN/GaN vertical-cavity lasers," in *Nitride Semiconductor Devices-Principles and Simulation*, edited by J. Piprek (Wiley-VCH, Weinheim, 2007), Chap. 19.
- ²¹J. Piprek and S. Nakamura, *IEE Proc.: Optoelectron.* **149**, 145 (2002).
- ²²T. C. Lu, T. T. Wu, S. W. Chen, P. M. Tu, Z. Y. Li, C. K. Chen, C. H. Chen, H. C. Kuo, S. C. Wang, H. W. Zan, and C. Y. Chang, *IEEE J. Sel. Top. Quantum Electron.* **17**, 1594 (2011).
- ²³E. Kioupakis, P. Rinke, K. T. Delaney, and Ch. G. Van de Walle, *Appl. Phys. Lett.* **98**, 161107 (2011).
- ²⁴J. Piprek, *Semiconductor Optoelectronic Devices* (Academic Press, San Diego, 2003), p. 56.
- ²⁵C.-Y. Huang, Y. D. Lin, A. Tyagi, A. Chakraborty, H. Ohta, J. S. Speck, S. P. DenBaars, and S. Nakamura, *J. Appl. Phys.* **107**, 023101 (2010).